Geofísica Internacional (2004), Vol. 43, Num. 2, pp. 173-186

Experimental observations of medium and small scale electrostatic waves associated with ionospheric electron density fluctuations

P. Muralikrishna, L. P. Vieira and M. A. Abdu
Instituto Nacional de Pesquisas Espaciais – INPE/MCT, São José dos Campos, SP, Brazil

Received: March 31, 2002; accepted: July 30, 2002

RESUMEN

El 18 de diciembre, 1995 a las 21:17 hrs (TL) se colocaron a bordo de la SONDA III brasileña una prueba de Langmuir y una de Capacitancia de Alta Frecuencia. Esta sonda fue lanzada desde la estación de lanzamiento de Alcantara (2.31°S; 44.4°W) en Brasil, para realizar mediciones de las variaciones con la altura del campo eléctrico ionosférico y de la densidad electrónica. La nave alcanzó una altitud de 557 km y cubrió un rango horizontal de 589 km. Se operaron desde tierra varios equipos para monitorear las condiciones ionosféricas durante el lanzamiento de modo que la nave alcanzara la región F, donde se presentan las burbujas de plasma. La nave alcanzó la altitud de 557 km y atravesó varias burbujas de plasma de mediano tamaño principalmente en donde se encuentra un perfil downleg de densidad. La densidad electrónica en la parte upleg del perfil mostró la presencia de una muy definida base de la región F alrededor de los 300 km, mientras que el downleg mostró la presencia de un amplio espectro de campo eléctrico e irregularidades en la densidad electrónica y el upleg de la capa F. El análisis espectral de las fluctuaciones en la densidad electrónica y el campo eléctrico indican la presencia de picos espectrales muy definidos a varias alturas que en la mayoría de los casos están asociados unos con otros. Probablemente esto indica la naturaleza electrostática de las ondas eléctricas que se excitan probablemente al inicio de la inestabilidad del plasma junto con las ondas de densidad. Se presentan algunos nuevos resultados de la asociación de estas fluctuaciones con las burbujas de plasma.

PALABRAS CLAVE: Ionosfera, observaciones de cohetes, campo electrónico ionosférico, densidad electrónica.

ABSTRACT

On 18 December, 1995 at 21:17 hrs (LT) an electric field double probe, a Langmuir probe, and a High Frequency Capacitance probe were flown from the equatorial rocket launching station Alcantara (2.31°S; 44.4°W) in Brazil on board a Brazilian SONDA III rocket, for measurements of the height variation of the ionospheric electric field and electron density. The rocket reached an apogee altitude of 557 km and covered a horizontal range of 589 km. Ground equipment monitored the ionospheric conditions during the launch. The rocket passed through several medium-scale plasma bubbles mainly during the downleg. The upleg electron density profile showed a clearly-defined base for the F-region around 300 km, while the downleg profile showed a wide spectrum of electric field and electron density irregularities in this height region as well as in the upper F-region. Spectral analysis of the fluctuations in electron density and electric field clearly indicated sharp spectral peaks at several heights, in most cases associated with each other. This is suggestive of the electrostatic nature of these E-field waves, that may be excited at the onset of plasma instabilities along with waves in electron density.

KEY WORDS: Ionosphere, rocket observations, ionospheric electric field, electron density.

1. INTRODUCTION

Electrostatic waves in the Earth's ionosphere exist over a large range of wavelengths, from centimeters to hundreds of kilometers, and over a large range of phase velocities, from quasi-static to speeds of hundreds of kilometers per second. Because of the motion of the spacecraft relative to ambient plasma, even quasi-static waves appear as fluctuations in the spacecraft frame. For electrostatic waves with frequencies below the ion plasma frequency or the lower hybrid frequency, both ions and electrons participate in the response of the medium to electrostatic waves. Thus electrostatic waves are expected to be associated with waves in electron density, or electron density irregularities.

Several linear and non-linear theories have been invoked to explain the wide spectrum of electron density irregularities observed in the nighttime F-region (Reid, 1968, Hudson *et al*., 1973, Sudan *et al*., 1973). Haerendal (1974) suggested a multi-step process to explain the large range of wavelengths observed, from several kilometers down to few centimeters. The collisional Rayleigh-Taylor (R-T) instability mechanism driven by gravity in the bottom side of the F-region gives rise to large plasma depletions or plasma bubbles.

The large density gradients associated with these rising bubbles are favorable for the operation of the gradient drift instability mechanism. Collisionless R-T instability mechanism is then invoked and kinetic drift waves grow upon these irregularities after they reach large amplitude. Chaturvedi and Kaw (1976) put forward a two-step theory of longer wavelength R-T modes directly coupling with kinetic collisional drift waves to explain the measured k^{-2} spectra of the electron density irregularities. Scannapieco and Ossakow (1976) from numerical simulation showed that the collisional R-T instability generated irregularities and bubbles on the bottom side of the F-region, which rose beyond the F-peak by Hall drift. This bubble phenomena were later confirmed by experimental observations of plasma density depletions (Kelly *et al*., 1976; McClure *et al*., 1977, Woodman and La Hoz, 1976). Analytical models for the rise of collisional and collisionless R-T bubbles were presented by Ott (1978).

It is now known that bubbles are mostly aligned with the geomagnetic field with plasma density decreases of up to 3 orders of magnitude. These depletions are generally produced over geomagnetic equator and they connect upwards through the F-layer peak to the topside ionosphere, reaching altitudes as high as 1200 km or more (Woodman and La Hoz, 1976). The post-sunset equatorial F-layer can become unstable under the influence of any disturbance produced by gravity waves, neutral winds or electric field fields, and can generate plasma irregularities through the R-T instability mechanism (Hysell *et al*., 1990, Singh *et al*., 1997). Steep plasma density gradients associated with the long wavelength R-T mode, create a condition which leads to the hierarchy of plasma instabilities giving rise to a wide spectrum of irregularities.

Electron density irregularities present in the ionosphere manifest themselves in different forms at different heights and times. Sporadic-E, spread-F, radio star scintillations and VHF radar echoes are a few of such phenomena, familiar to ionospheric physicists. Basic knowledge of the plasma irregularities, responsible for these phenomena, has progressed considerably, both in theory and observations, since the discovery of the strong VHF radar echoes from the equatorial ionosphere (see Bowles *et al*., 1963 and Balsley, 1969), from their spectral characteristics as observed by the VHF radar, classified the plasma irregularities into two groups, namely Type I and Type II. While the Type I irregularities are now identified to be consistent with the two-stream instability mechanism (Farley, 1963), the Type II irregularities are known to be produced by the nonlinear cross-field instability mechanism (see Rogister and d'Angelo, 1972; Balsley and Farley, 1973). Direct observations by Prakash *et al*. (1970) using rocket-borne Langmuir probes flown from India, confirm the existence of the Type II irregularities in the equatorial E-region. Type II irregularities are characterized by scale sizes extending from a few meters upto tens of kilometers. The short wavelength irregularities apparently seem to be generated from larger scale sizes through nonlinear coupling or cascading processes (see Rogister and d'Angelo, 1972; Sato 1973; Sudan *et al*., 1973). Neutral turbulence also seems to be another probable mechanism responsible for the generation of plasma irregularities (Prakash *et al*., 1970). The spectral characteristics of the different types of irregularities have been studied in detail (Prakash *et al*., 1970; Ott and Farley, 1974).

Five major rocket campaigns have been reported for studying the phenomenon of spread-F in the American region (Kelly *et al*., 1976, Morse *et al*., 1977, Rino *et al*., 1981; Szuszczewicz *et al*., 1981, Kelley *et al*., 1982; Hysell *et al*., 1994) and a few campaigns in the Indian zone (Raghavarao *et al*., 1987; Prakash *et al*., 1991). From simultaneous *in situ* measurements of electron density and electric field fluctuations Hysell *et al*. (1994) showed that irregularities in the scalesize range of 100 m- 2 km display a power law behavior with spectral index $n \approx -2$ that increased to –4.5 for wavelength around 100 m and below when F-layer is high.

The effective linear growth rate for the irregularities generated through the Generalized Rayleigh-Taylor (GRT) instability mechanism including the effect of vertical winds can be written as:

$$\gamma_g = \frac{g}{\nu_{in} L} - \frac{E}{BL} - \frac{U}{L} - \frac{W}{L} - \eta_R \ ,$$

where g is the acceleration due to gravity, U and W respectively are the horizontal and vertical components of the neutral wind (taken positive upward and eastward), ν_{in} is the ion neutral collision frequency, L is the gradient scale length (taken positive upward), E is the horizontal electric field (taken positive eastward) and η_R is the recombination coefficient. As can be seen from this relation, when L is positive (base of the F-region for example), westward electric field and a neutral wind with downward and westward components will increase the growth rate of the R-T irregularities.

The gradient-drift or cross-field instability mechanism occurs in regions where E is parallel to the electron density gradient (Reid, 1968; Tsuda *et al*., 1969). In other words height regions where E and L have the same sign are favorable for the generation of irregularities by this mechanism. As mentioned earlier the steep electron density gradients associated with the plasma bubbles produced by the collissional or noncollisional R-T instability creates conditions favorable for the generation of smaller scale size irregularities by the gradient-drift and other instability mechanisms. The spectral indices as well as the exact relationship

between the electron density and electric field fluctuations depends on the type and the scale size of irregularities. Measurement of these parameters, thereby, can give us valuable information on the plasma instability mechanism responsible for the generation of these irregularities.

With the above objective *in situ* measurements of the height variation of the ionospheric electric field and electron density variations were made with a rocket-borne electric field double probe and two different types of electron density probes. A Brazilian made SONDA III rocket carrying these experiments in addition to other airglow experiments was launched on 18 December, 1995 at 21:17 hrs (LT) from the equatorial rocket launching station, Alcantara (2.31°S; 44.4°W) in Brazil. The rocket reached an apogee altitude of 557 km and covered a horizontal range of 589 km. Several ground equipments were operated during the launch campaign with the specific objective of knowing the ionospheric conditions at the time of launch and thereby to launch the rocket into an F-region prone to the presence of plasma bubbles.

Specific attempts were made to look into the possible existence of sharp spectral lines in the spectral distribution of irregularities in electron density and electric field, associated with developing plasma bubbles. The results obtained from comparative study of the spectral features of the electron density and electric field fluctuations are presented in this paper.

2. EXPERIMENT AND FLIGHT DETAILS

The rocket payload designated IONEX-II, shown schematically in Figure 1 had the principal objective of measuring the electric field, the electron density, the electron kinetic temperature and the spectral distribution of plasma irregularities associated with what are known as ionospheric plasma bubbles. The payload consisted of the following experiments in addition to other airglow photometers.

- Electric Field Double Probe (EFP)
- Langmuir Probe (LP)
- High Frequency Capacitance probe (HFC)

Electric Field Double Probe (EFP)

The main objective of the EFP was to measure the dc electric field and the fluctuating component of it associated with the ionospheric plasma irregularities. Two spherical electric field sensors of 60 mm diameter were mounted at the extremities of two booms, each about 50 cm long, that were deployed after the rocket nosecone was ejected at an altitude of about 65 km. Though, in the fully deployed state the separation between the electric field sensors was expected to be more than 3 m, the booms did not open fully due to the unexpectedly low spin rate (less than the expected 3 rps) attained by the rocket and the separation between the sensors obtained was only about 1.3 m. This made the already difficult task of obtaining the dc component of the electric field practically impossible. However the ac component of the electric field in a plane perpendicular to the spin axis of the rocket could be measured in the altitude region of about 95 to 557 km, the apogee altitude reached by the rocket and are being analyzed.

Langmuir Probe (LP)

A Langmuir Probe was used to measure the electron density and the electron kinetic temperature. A spherical LP sensor of diameter 60 mm was mounted at the extremity of a short boom of about 50 cm in length that remained inside the rocket nosecone. This boom was deployed along with the EFP booms soon after the ejection of the rocket nosecone. A sweep voltage varying from -1V to +2.5 V in about 2.5 sec. was applied to the LP sensor in order to measure both the electron density and the electron kinetic temperature.

High Frequency Capacitance Probe (HFC)

The main objective of the HFC probe was to measure the electron density height profile. The HFC sensor was identical to the LP sensor and was mounted also at the extremity of a short 50 cm boom kept folded inside the rocket nosecone till the ejection of the nosecone like the LP sensor boom. The sensor formed part of the tank circuit of an electronic oscillator and any change in the sensor capacitance caused by changes in the ambient electron density, is measured through a counting circuit and this information is telemetered to the ground.

The basic principle of operation and the details of the electronic subsystem of the LP and HFC experiments are given in Muralikrishna and Abdu (1991). The mounting of the electric field booms and the booms carrying the LP and HFC sensors inside the rocket nosecone is shown in Figure 1.

3. RESULTS AND DISCUSSION

The electron density profiles estimated from the LP and HFC data for the rocket upleg and downleg are shown in Figures 2 and 3. The general features of the two sets of electron density profiles are very similar, though the absolute values of the electron densities at different height regions show considerable differences. Muralikrishna and Abdu (1991) tried to explain similar differences observed in one

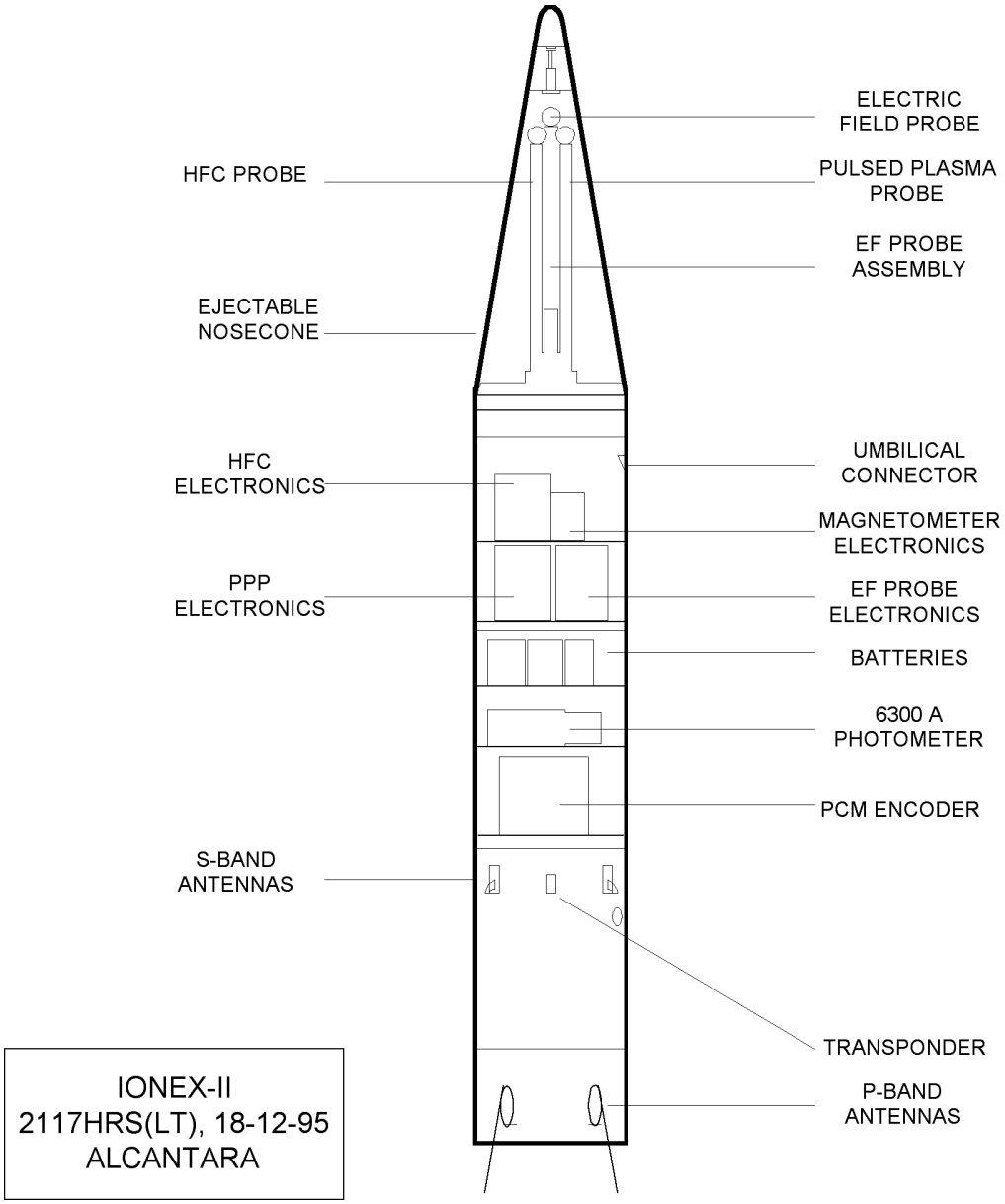

Fig. 1. Payload bay of the rocket SONDA III showing the mounting of the different experiments.

of their earlier *in situ* measurement as due to certain inherent problem associated with the two techniques of measurement. However what is more important in the present studies is the relative variation of the electron density with altitude. As can be seen from figures 2 and 3 the upleg profile shows the presence of a rather steep F region base, free of any large scale electron density depletions or bubbles, while the downleg profile shows the presence of a large number of plasma bubbles. The F-region base observed during the rocket downleg shows the presence of a few large plasma depletions or bubbles and does not exhibit a sharp nature as observed during the rocket upleg. Intense spread-F traces were seen in the ionograms during this period.

The electron density and the electric field fluctuation data were sampled at a rate of 1250 per second and this decided the lower limit for the measurable scale size. The maximum observable fluctuation frequency is 625 Hz. This corresponds to different scale sizes at different height regions because of the continuously changing rocket speed. For example in the height region where the rocket velocity is about 2 km per second the LP and EFP experiments could measure the ac fluctuations of wavelength down to about 3,2 m. Close to the region of apogee where the vertical component of the rocket velocity is very small the lowest vertical scale size of irregularities that can be measured with the LP and EFP goes down to practically zero.

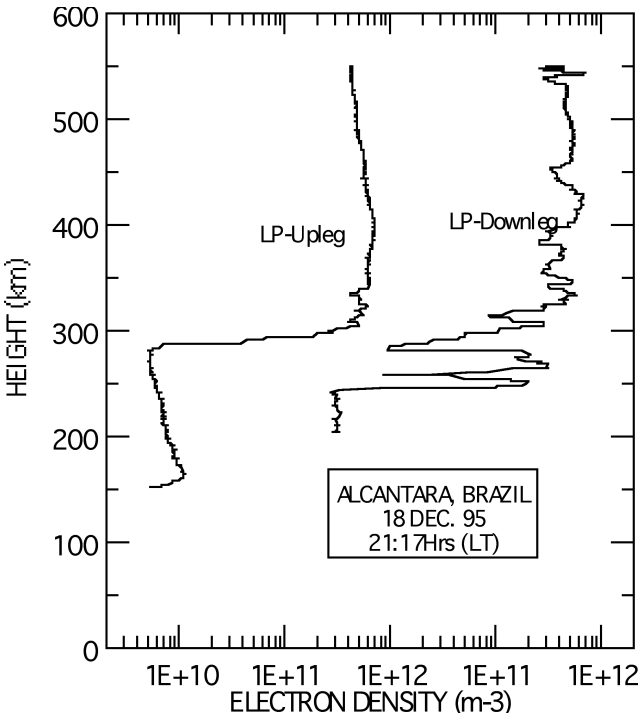

Fig. 2. LP Upleg and downleg electron density profiles showing the presence of a large number of plasma bubbles especially in the downleg profile.

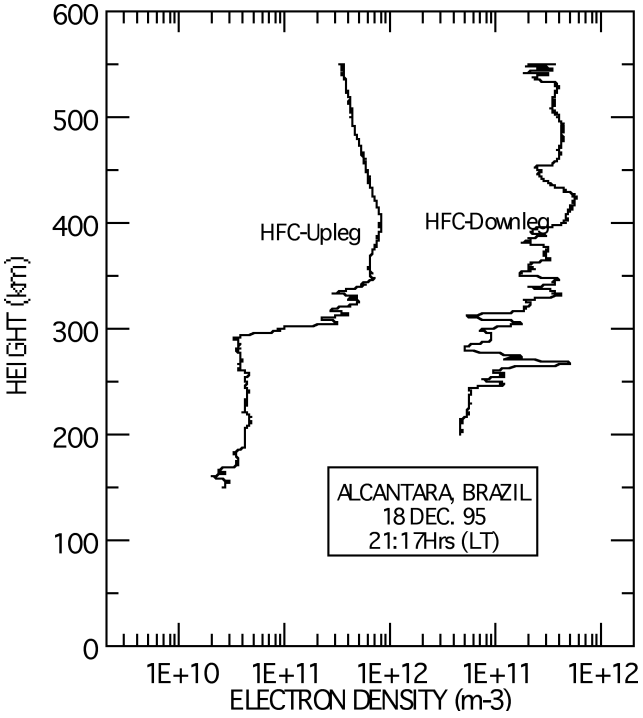

Fig. 3. HFC Upleg and downleg electron density profiles showing features similar to those seen in the LP profiles.

Fluctuating parts of the electron density measured by the LP and the electric field measured by the EF experiments are separated from the dc variations using a high pass filter with 3 db cut-off frequency at about 10 Hz. An FFT algorithm was then used to estimate the spectral characteristics of these fluctuations. It should be noted here that the LP and EF sensors were mounted away from the rocket body in a plane perpendicular to the rocket spin axis. The electric field measured thus represents only the component of the field perpendicular to the spin axis of the rocket. The rocket had a spin rate of less than 3 per second which in fact can be clearly seen in the total electric field data, but the amplitude of this modulation is reduced very much in the electric field fluctuation data that is separated through the high pass filter. The effect of rocket spin on the electron density data given by the LP is rather negligible. The fluctuating components of the LP and EF data corresponding to the time intervals when the LP sensor is in saturation current mode (at +2.5 V bias) only are chosen for the present analysis. The EF data chosen also correspond to the same intervals of time. For spectral analysis three sets of data are chosen corresponding to selected height regions for both the upleg and downleg of the rocket.

The conventional power spectra (known as k-spectra) of the electron density (n_e) and electric field fluctuations observed at selected height regions during the rocket upleg and downleg are shown in Figures 4 to 7. The spectral indices estimated for each spectrum for lower and higher wavenumbers separately are also indicated in the figures. The spectral indices observed are mostly in conformity with what are expected from theoretical considerations of GRT and other instability mechanisms briefly explained earlier. What is to be noted here is the striking similarity between the spectral features of the electron density and electric field fluctuations indicating that the waves observed in the electric field are in fact small and medium scale electrostatic waves. However the conventional k-spectra do not indicate the presence of any preferred spectral lines in neither the electron density nor the electric field fluctuations. An attempt is made here to look into this aspect of the spectra.

Figures 8 to 14 show the amplitude spectra of the electron density and electric field fluctuations in arbitrary units corresponding to different height regions selected from the upleg and down leg trajectories of the rocket. Each spectrum is estimated from a data block containing 1024 points collected in about 0.8 seconds. It should be noted here that the x-axis on which the data sequence from 1 to 512 is plotted, therefore represents frequency in the time domain or wave number k in the space domain. This can be converted to frequency knowing that sampling rate of the data is 1250/sec, and later to wave number k knowing the rocket speed at the specific height chosen. The spectral amplitude is shown along the y-axis and has an arbitrary scale. There are three

Fig. 4. Conventional Power Spectra of ($\delta n_e/n_e$) versus wavenumber k showing the spectral index at selected heights for rocket upleg.

sets of data shown, denoted by (a), (b) and (c), and the mean height corresponding to each set is also shown. In each set of data the top one represents the spectral features of n_e and the bottom one those in the E field. Since the n_e and E sensors are mounted at the extremities of booms of about 50 cm length that are deployed on to a plane perpendicular to the spin axis of the rocket, one would expect a large spin modulation in the E field, and little effect of the spin modulation in n_e. The rocket spin as measured by the on board magnetometers was less than 2.5 per second. This modulation is seen in the data, especially the E field data.

From a close look at Figure 8, one can see the existence of sharp spectral lines in a rather continuous background

Fig. 5. Conventional Power Spectra of δE versus wavenumber k showing the spectral index at selected heights for rocket upleg.

in both the n_e and E-field spectra. Not only that they appear at the same frequencies in both the spectra, but also their relative amplitudes are approximately same. Being accompanied by corresponding fluctuations in n_e, these E-field fluctuations seem to be electrostatic in nature and therefore may be derived from a scalar potential. The spectral lines are seen in all the three samples presented here.

A close examination of the spectral features of fluctuations in n_e and E-field shown in Figure 9 also shows the presence spectral lines common to both the electron density and electric field fluctuations.

The spectral characteristics of the n_e and E-field fluctuations in the region above the F-peak are shown in Figure

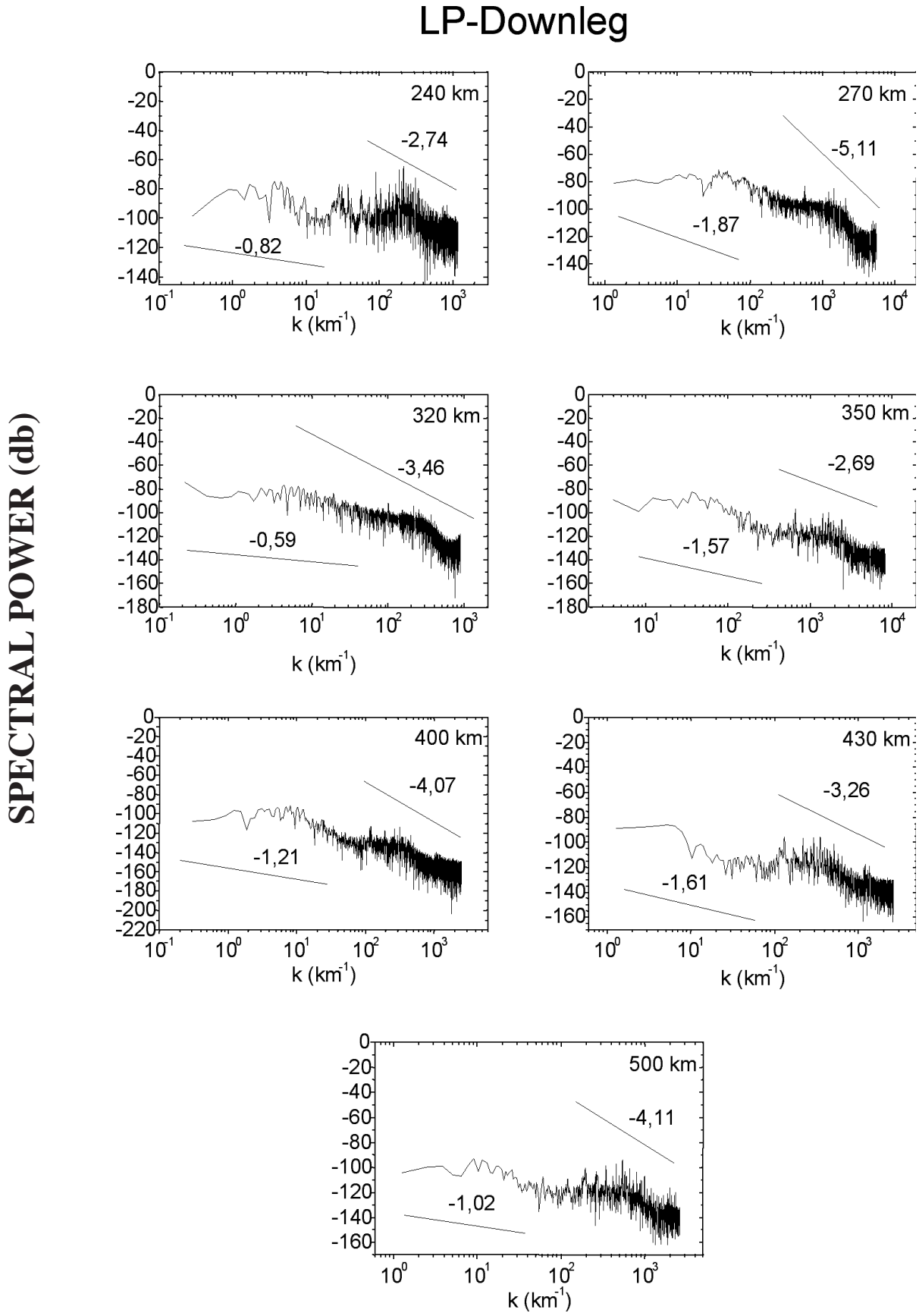

Fig. 6. Conventional Power Spectra of ($\delta n_e/n_e$) versus wavenumber k showing the spectral index at selected heights for rocket downleg.

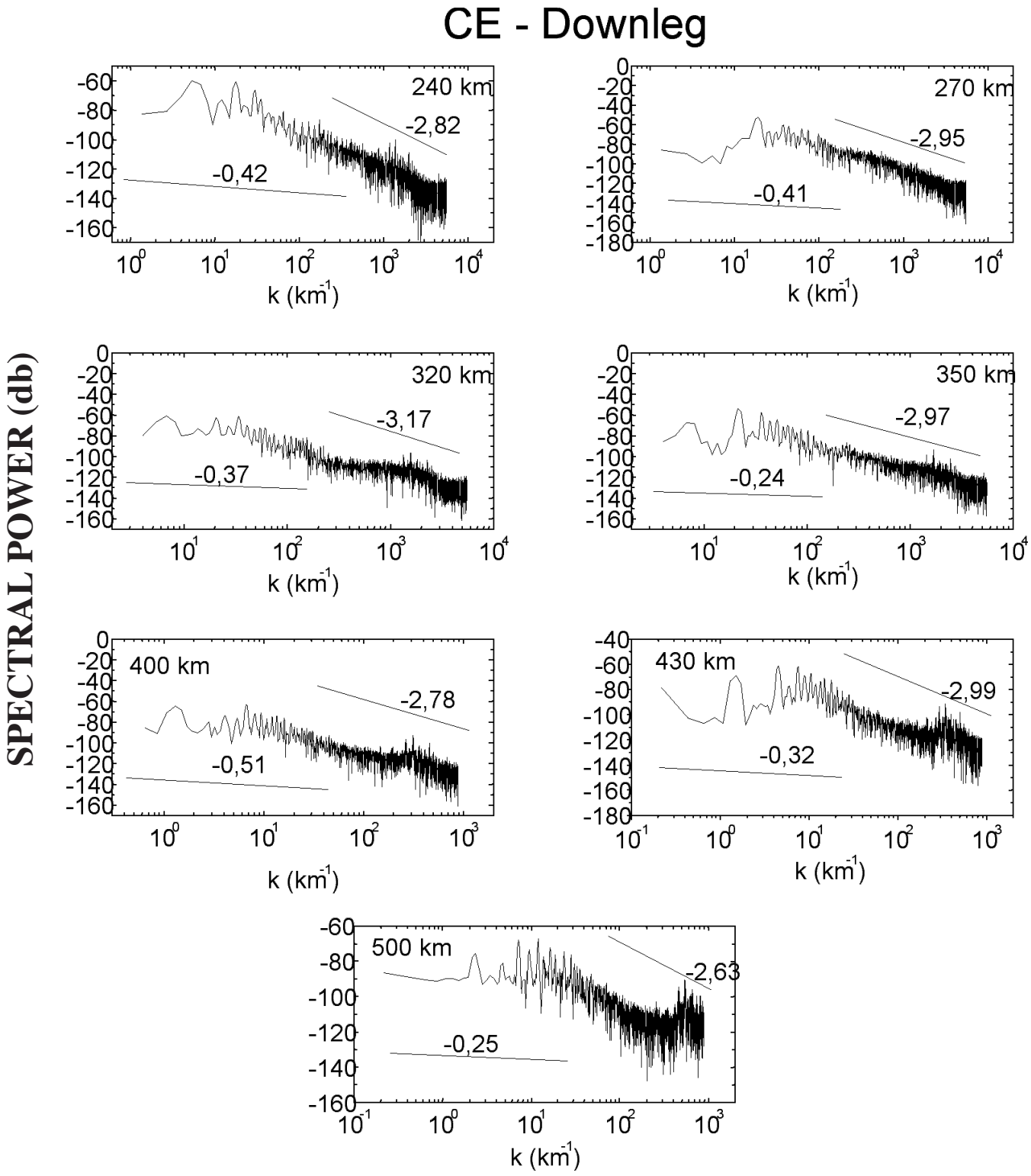

Fig. 7. Conventional Power Spectra of δE versus wavenumber k showing the spectral index at selected heights for rocket downleg.

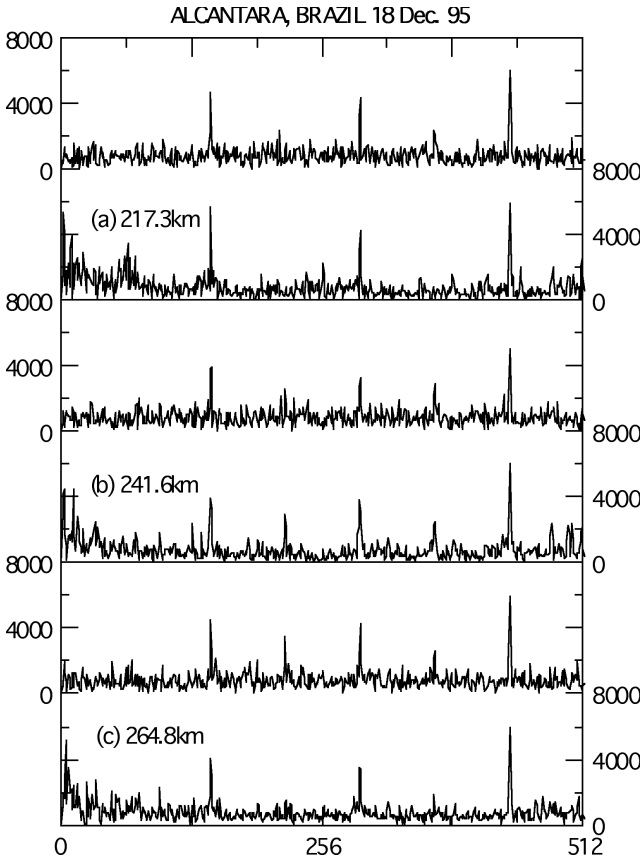

Fig. 8. Spectral amplitudes of electron density (top) and electric field (bottom) fluctuations in the height regions of (a) 217.3 km, (b) 241.6 km, and (c) 264.8 km for rocket upleg.

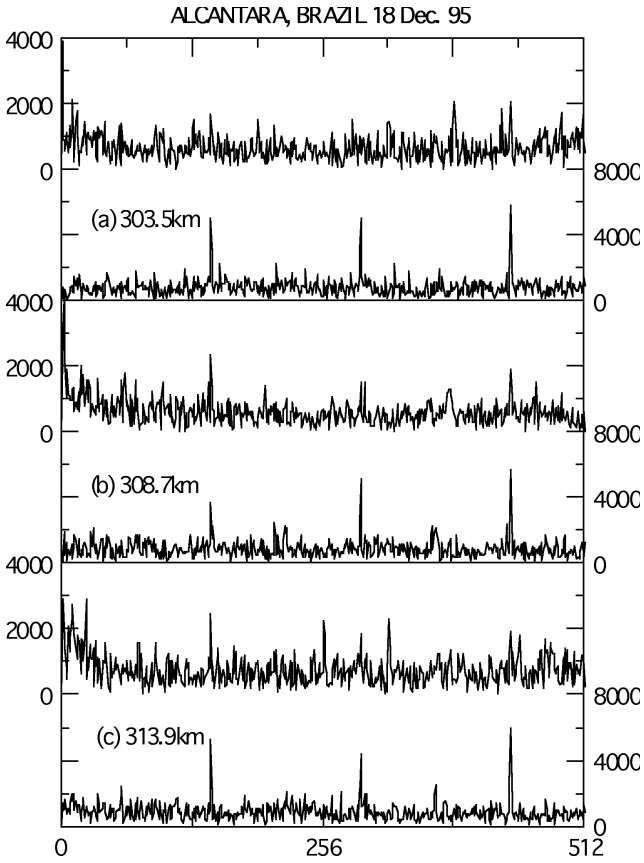

Fig. 9. Spectral amplitudes of electron density (top) and electric field (bottom) fluctuations in the height regions of (a) 303.5 km, (b) 308.7 km, and (c) 313.9 km for rocket upleg.

10. One should remember here that the electron density profile observed during the upleg of the rocket does not indicate the presence of neither plasma bubbles nor large or medium scale plasma irregularities. However the downleg profile indicates the presence of a large number of plasma bubbles and associated large, medium and small-scale irregularities. The spatial and temporal separation of the upleg and downleg trajectories of the rocket being small, the rather complete absence of plasma bubbles in the upleg profile and the presence of a large number of bubbles in the downleg profile indicate that the bubbles could be recently generated and be in their developing phase. The characteristic features of the electron density and E-field spectra inside and outside these bubbles may provide us with valuable information about the irregularities associated with plasma bubbles and their growth process.

Three samples of n_e and E-field spectra observed during the rocket downleg at the selected heights of 421.9 km, 397.9 km, and 385.2 km are shown in Figure 11. The spectral data show that there are no dominant spectral lines present. In other words the medium and small scale irregularity amplitudes are rather low in these altitudes. As can be seen from Figure 12, where the spectral data corresponding to 376.2 km, 367.2 km and 358.0 km altitudes are shown, the energy is rather uniformly distributed at all frequencies and there are no dominant spectral lines at 376.2 km, while at the other two altitudes a considerable part of the wave energy is concentrated in a few spectral lines. As can be seen from Figure 13, the wave energy is more or less uniformly distributed at all the frequencies at altitudes 348.4 km and 328.8 km (no sharp spectral lines are seen), and at 338.7 km there exist a few sharp spectral lines that share a considerable part of the wave energy. At the altitude of 308.2 km (Figure 14) most of the energy is shared by a few sharp spectral lines, while at the other two altitude regions the wave energy is rather uniformly distributed in a wide range of wavelengths.

Thus the important aspects of the spectral features presented in Figures 8 to 14 can be summarized as given below.

- At most of the heights the spectral data show the presence of sharp spectral lines in both n_e and E. This probably

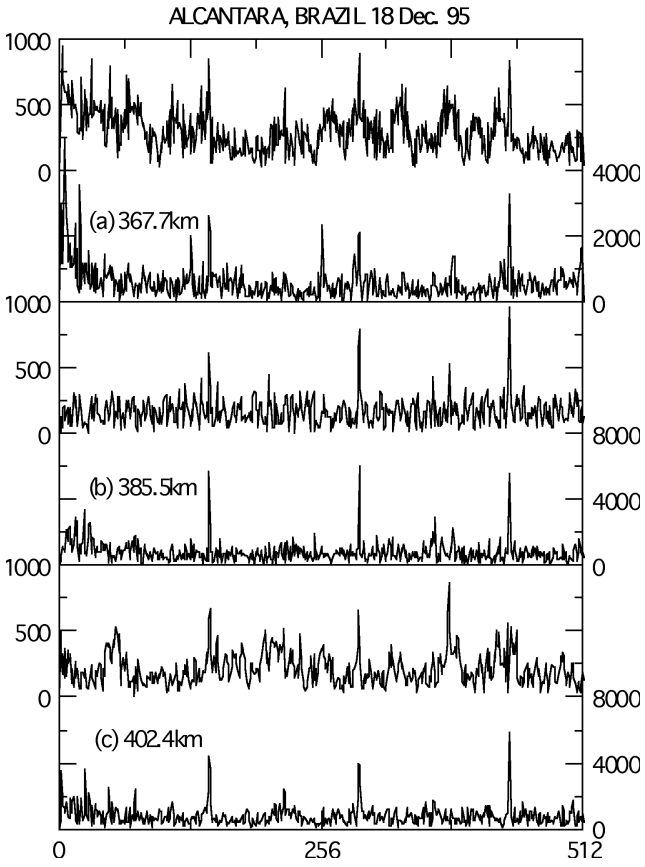

Fig. 10. Spectral amplitudes of electron density (top) and electric field (bottom) fluctuations in the height regions of (a) 367.7 km, (b) 385.5 km, and (c) 402.4 km for rocket upleg.

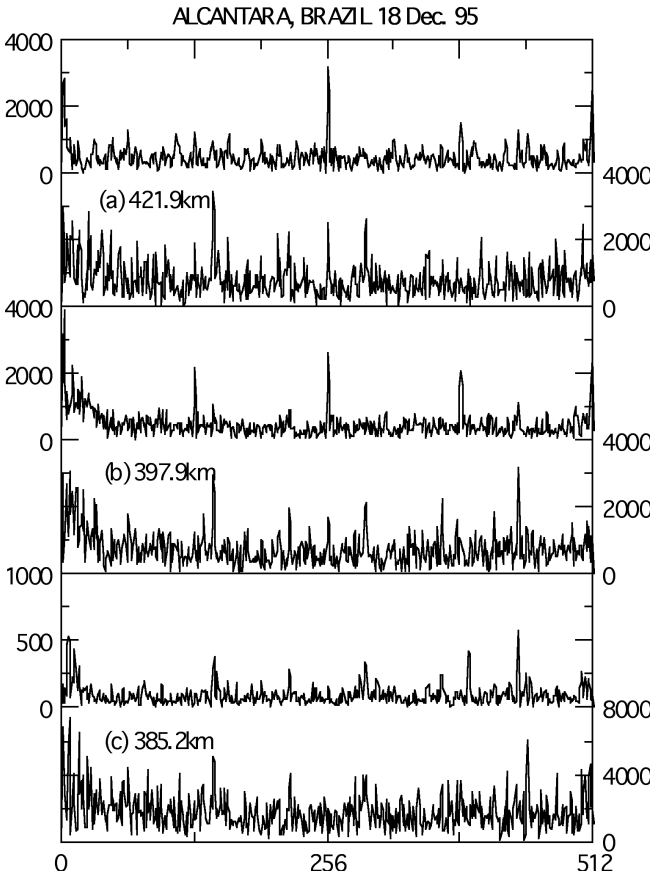

Fig. 11. Spectral amplitudes of electron density (top) and electric field (bottom) fluctuations in the height regions of (a) 421.9 km, (b) 397.9 km, and (c) 385.2 km for rocket downleg.

shows the development of some instability mechanism, which are characterized by waves in both n_e and E-field. These waves, in course of time, break into smaller scale waves (cascade process) losing part of their energy. This may finally lead to a steady state distribution (without spectral peaks) of energy in a large range of wavelengths. This final state maybe characterized by one or more characteristic spectral indices for the irregularities reported in the literature.

- At those height regions where no spectral peaks are observed neither in n_e nor in E-field, and their fluctuation amplitudes are relatively high, the situation has already reached a steady state, wherein the spectral features are those that are expected from the existing theories.

- At those heights where no spectral lines are observed, and the fluctuation amplitudes are also relatively low, the physical conditions seem to be unfavorable for the operation of the plasma instability mechanisms.

All the cases reported here and presented in Figures 4 to 10 can be classified into one of the above three cases.

The present observation of electrostatic waves in the ionosphere clearly shows that electric field double probes can also be used to detect $\delta\mathbf{E}$ fluctuations associated with electrostatic waves. Although both spherical and cylindrical sensors can be used to detect these waves, in general, double probes that employ spherical sensors are better suited for detecting electrostatic modes, particularly for low frequency, short scale waves. To determine the instantaneous vector $\delta\mathbf{E}$ components from three orthogonally oriented double probes must be obtained simultaneously.

CONCLUSIONS

- Bubble regions are associated with a wide spectrum of both electron density and electric field fluctuations which, from their spectral characteristics, can be attributed to the GRT and gradient drift instability mechanisms.

- The electric field fluctuations are associated with electrostatic waves and thereby are associated with similar fluctuations in the ambient electron density.

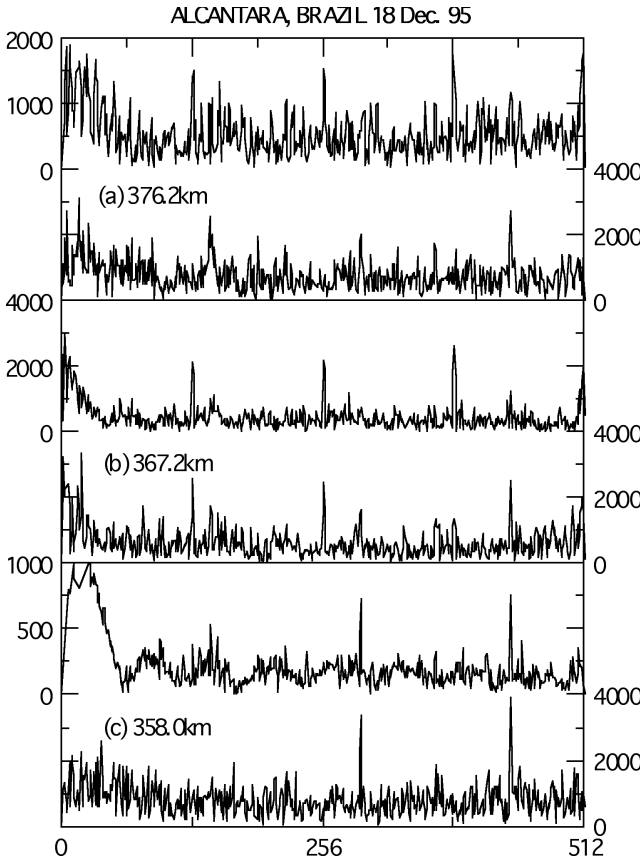

Fig. 12. Spectral amplitudes of electron density (top) and electric field (bottom) fluctuations in the height regions of (a) 376.2 km, (b) 367.2 km, and (c) 358.0 km for rocket downleg.

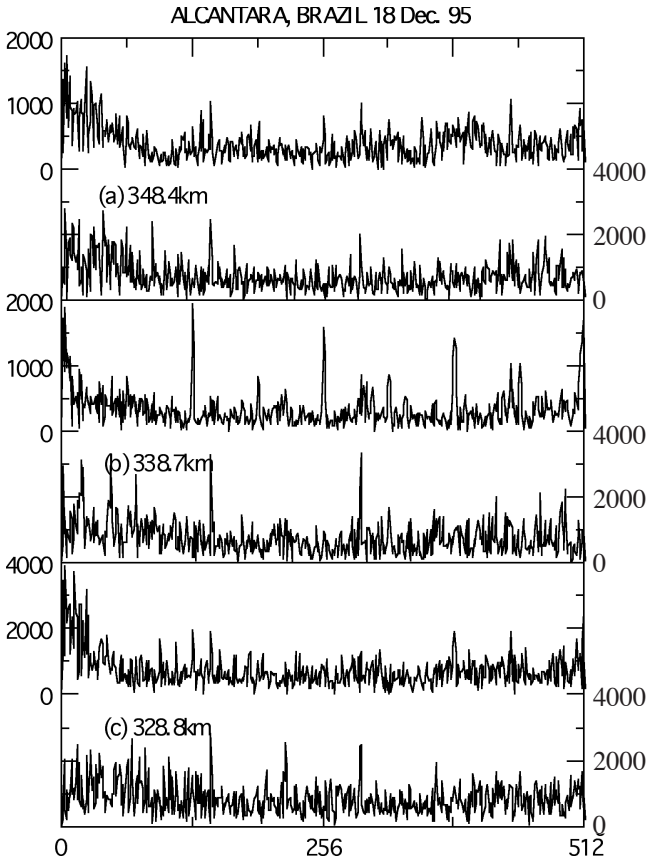

Fig. 13. Spectral amplitudes of electron density (top) and electric field (bottom) fluctuations in the height regions of (a) 348.4 km, (b) 338.7 km, and (c) 328.8 km for rocket downleg.

- The observation of sharp spectral lines in the n_e and/or E-field spectra indicate the development phase of some plasma instability mechanism.

- The absence of sharp spectral lines in n_e and/or E-field probably indicates that the cascading process of the generation irregularities has already reached the final state or that the physical conditions in the particular height region are not favorable for the operation of any plasma instability mechanism.

5. ACKNOWLEDGMENTS

The authors are grateful to the Directors of IAE/CTA and CLA, Alcantara for providing the rockets and the launch facilities respectively and to the staff of IAE and CLA for their help during the pre-launch tests of the experiments, and during the launching of the rockets. Sincere thanks are to Sinval Domingos, Agnaldo Eras and Narli Baesso Lisboa for their technical help in the development testing and integration of the experiments. The work reported here was partially supported by FINEP under contract FINEP-537/CT, and by CNPq under process 300253/89-3/GM/FV. The authors are grateful to the Organizing Committee of VI COLAGE, which extended financial assistance for the presentation of this work during the VI COLAGE Meeting held at Tomé, Chile during 1-5 October, 2001.

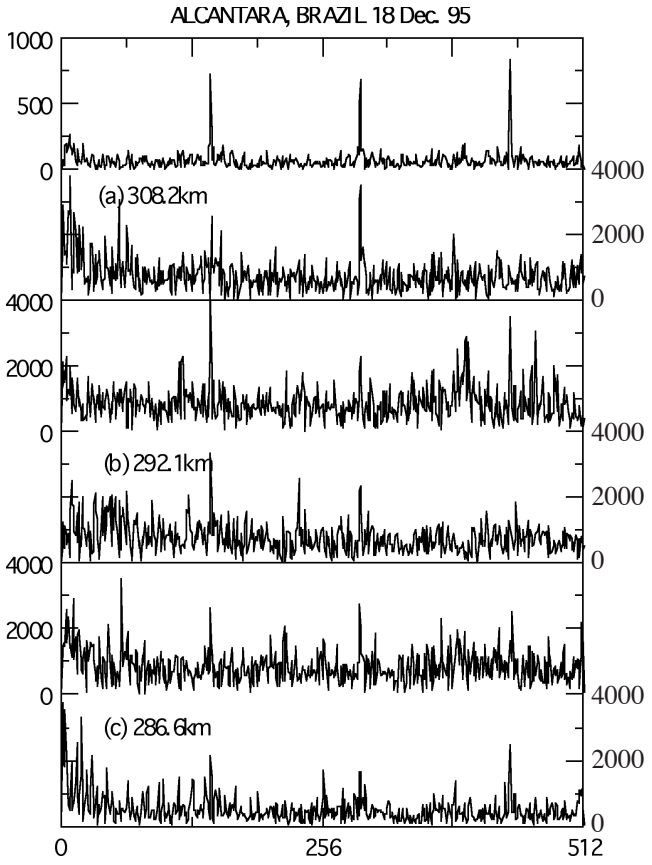

Fig. 14. Spectral amplitudes of electron density (top) and electric field (bottom) fluctuations in the height regions of (a) 308.2 km, (b) 292.1 km, and (c) 286.6 km for rocket downleg.

6. BIBLIOGRAPHY

BALSLEY, B.B., 1969. Some characteristics of non two-stream irregularities in the equatorial electrojet. *J. Geophys. Res , 74*, 2333.

BALSLEY, B. B. and D. T. FARLEY, 1973. Radar observation of two-dimensional turbulence in the equatorial electrojet. *J. Geophys. Res., 78,* 7471-7479.

BOWLES, K. L., B. B. BALSLEY and E. COHEN, 1963. Field- aligned E-region irregularities identified with ion acoustic waves. *J. Geophys. Res , 68*, 2485.

CHATURVEDI, P. K. and P. KAW, 1976. An interpretation for the power spectrum of spread-F irregularities. *J. Geophys. Res., 81*, 3257-3260.

FARLEY, D. T., 1963. A plasma instability resulting in field aligned irregularities in the ionosphere. *J. Geophys. Res., 68,* 6083.

HAERENDAL, G., 1974. Theory of equatorial spread-F, Report of Max Planck Institut für Physik und Astrophysik, Garching, Germany.

HUDSON, M. K., C. F. KENNEL and P. K. KAW, 1973. Two step drift mode theory of equatorial spread-F. *Trans. Am. Geophys. Soc., 54,* 1147.

HYSELL, D., M. C. KELLEY, W. E. SWARTZ, R. F. PFAFF and C. M. SWENSON, 1990. Seeding and layering of equatorial spread-F by gravity waves. *J. Geophys. Res., 95*, 17253-17260.

HYSELL, D., M. C. KELLEY, W. E. SWARTZ and R. F. WOODMAN, 1994. Steepened structures in equatorial spread-F, 1. New observations. *J. Geophys. Res., 99,* 8827-8840.

KELLY, M. C., G. HAERENDAL, H. KAPPLER, A. VALENZUELA, B. B. BALSLEY, D. A. CARTER, W. L. ECKLUND, C. W. CARLSON, B. HAUSLER and R. TORBERT, 1976. Evidence for a Rayleigh Taylor type instability and upwelling of depleted density regions, during equatorial spread-F. *Geophys. Res. Letts., 3*, 448-450.

KELLEY, M. C., R. C. LIVINGSTON, C. L. RINO and R. T. TSUNODA, 1982. The vertical wavenumber spectrum of topside equatorial spread-F: Estimates of backscatter levels and implications for a unified theory. *J. Geophys. Res., 87*, 5217.

MCCLURE, J. P., W. B. HANSON and J. H. HOFFMAN, 1977. Plasma bubbles and irregularities, in the equatorial ionosphere. *J. Geophys. Res., 82,* 2650-2656.

MORSE, F. A., B. C. EDGAR, H. C. KOONS, C. J. RICE, W. J. HEIKKILA, J. H. HOFFMAN, B. A. TINSLEY, J. D. WINNINGHAM, A. B. CHRISTENSEN, R. F. WOODMAN, J. POMALAZA and R. N. TEIXEIRA, 1977. Equion, an equatorial ionospheric irregularity experiment. *J. Geophys. Res., 82*, 578.

MURALIKRISHNA, P. and M. A. ABDU, 1991. In-situ measurement of ionospheric electron density by two different techniques - a comparison. *J. Atmos. Terr. Phys., 53,* 787-793,

OTT, E., 1978. Theory of Rayleigh-Taylor bubbles in the equatorial ionosphere. *J. Geophys. Res., 83,* 2066-2070.

OTT, E. and D. T. FARLEY, 1974. The k-spectrum of ionospheric irregularities. *J. Geophys. Res., 79,* 2469-2472.

MORSE, F. A., B. C. EDGAR, H. C. KAONS, C. J. RICE, W. J., HEIKKILA, J. H. HOFFMAN, B. A. TINSLEY, J. D. WINNINGHAM, A. B. CHRISTENSEN, R. F. WOODMAN, J. POMALAZA, and R. N. TEIXEIRA, 1977. Equion, an equatorial ionospheric irregularity experiment. *J. Geophys. Res., 82*, 578.

PRAKASH, S., S. P. GUPTA and B. H. SUBBARAYA, 1970. A study of irregularities in the nighttime equatorial E-region using a Langmuir probe and a plasma noise probe. *Planet. Space Sci. 18,* 1307-1318.

PRAKASH, S., S. PAL and H. CHANDRA, 1991. *In situ* studies of equatorial spread-F over SHAR- steep gradients in the bottomside F-region and transitional wavelength results. *J. Atmos. Terr. Phys., 53,* 977-986.

RAGHAVARAO, R., S. P. GUPTA, R. SEKAR, R. NARAYANAN, J. N. DESAI, R. SRIDHARAN, V. V. BABU and V. SUDHAKAR, 1987. *In situ* measurements of wind, electric fields and electron densities at onset of equatorial spread-F. *J. Atmos. Terr. Phys., 49,* 485-492.

REID, G. C., 1968. Small scale irregularities in the ionosphere. *J. Geophys. Res., 73,* 1627-1640.

RINO, C. L., R. T. TSUNODA, J. PETRICEKS, R. C. LIVINGSTON, M. C. KELLEY and K. D. BAKER, 1981. Simultaneous rocket-borne beacon and *in situ* measurements of equatorial spread-F. *J. Geophys. Res., 86,* 2411.

ROGISTER, A. and N. D'ANGELO, 1970. Type 2 irregularities in the equatorial electrojet. *J. Geophys. Res., 75*, 3819.

SATO, T., 1973, A unified theory of Type I and II irregularities in the equatorial electrojet. *J. Geophys. Res., 78,* 2232-2243.

SCANNAPIECO, A. J. and S. L. OSSAKOW, 1976. Nonlinear equatorial spread-F. *Geophys. Res. Letts., 3*, 451-454.

SINGH, S., D. K. BHAMGBOYE, J. P. MCCLURE and F. S. JOHNSON, 1997. Morphology of equatorial plasma bubbles. *J. Geophys. Res., 102*, 20019-20029.

SUDAN, R.N., J. AKINRIMISI and D. T. FARLEY, 1973. Generation of small scale irregularities in the equatorial electrojet. *J. Geophys. Res., 78,* 240.

SZUSZCZEWICZ, E. P., R. T. TSUNODA, R. NARCISI and J. C. HOLMES, 1981. Plumex II: A second set of coincident radar and rocket observations of equatorial spread-F. *Geophys. Res. Letts., 8,* 803-806.

TSUDA, T., T. SATO and S. MATSUSHITA, 1969. Ionospheric irregularities and cross-field plasma instability. *J. Geophys. Res., 74*, 2923-2932.

WOODMAN, R. F. and C. LA HOZ, 1976. Radar observations of equatorial F-region irregularities. *J. Geophys. Res., 81*, 5447-5466.

———

P. Muralikrishna, L. P. Vieira and M. A. Abdu
Instituto Nacional de Pesquisas Espaciais – INPE/MCT
C. P. 515, 12 201-970, São José dos Campos - SP, Brazil.
Email: murali@dae.inpe.br